



Halogenated azobenzene acrylates: from efficient solution photoswitching to stable solid-state photochromic materials

Martina Vachtlová¹, Michaela Fecková¹, Vítězslav Zima², Jan Podlesný^{*1}, Milan Klikar³, Oldřich Pytela³, Patrik Pařík³, Jakub Opršal², Eliška Juhaňáková¹, Veronika Chrtová¹ and Filip Bureš^{*3}

Full Research Paper

Open Access

Address:

¹Institute of Technology and Business in České Budějovice, Okružní 517/10, České Budějovice, 37001, Czech Republic, ²Synpo, a. s., S. K. Neumannova 1316, Pardubice, 53002, Czech Republic and ³Institute of Organic Chemistry and Technology, Faculty of Chemical Technology, University of Pardubice, Studentská 573, Pardubice, 53210, Czech Republic

Email:

Jan Podlesný* - podlesny@vste.cz; Filip Bureš* - filip.bures@upce.cz

* Corresponding author

Keywords:

azobenzene; *E/Z* isomerization; halogen; photoswitch; polymer; thin film

Beilstein J. Org. Chem. **2026**, *22*, 782–794.

<https://doi.org/10.3762/bjoc.22.60>

Received: 11 February 2026

Accepted: 08 May 2026

Published: 21 May 2026

This article is part of the thematic issue "π-Conjugated molecules and materials".

Guest Editor: A. Mateo-Alonso



© 2026 Vachtlová et al.; licensee Beilstein-Institut.
License and terms: see end of document.

Abstract

The design, synthesis, and comprehensive characterization of six novel halogenated azobenzene acrylate monomers bearing fluorine, chlorine or bromine substituents is reported. The monomers were prepared via a facile three-step synthetic route involving azo-coupling, *O*-alkylation and *O*-acylation. Apart from the steady electrochemical properties, halogen substitution proved to be a very useful tool to tune the thermal and optical properties, light-induced switching in particular. Monohalogen derivatives exhibited up to 93% *E* → *Z* photoconversion efficiency in solution, whereas the efficiency of dihalogen analogues is lower by 20%, which is ascribed to their nonplanar arrangement. Kinetics studies identified the most stable *Z*-isomer of the difluoro derivative ($\tau_{1/2} = 3.74/6.59$ h at 60 °C in DCE/ CDCl_3). The monofluoro derivative embedded in a polystyrene film demonstrated photoresponsive behavior and remarkable stability by maintaining a macroscopically visible color change for over 90 days. These findings demonstrate that *ortho*-halogenation is a powerful tool for tuning the properties of photoresponsive materials for potential applications in colorimetric thermal sensing and light-controlled functional systems.

Introduction

The azobenzene photoinduced *E/Z* isomerization represents a well-investigated switching process that found various utilizations [1-4]. In contrast to the state-of-the-art achieved in solu-

tion and despite its perhaps even greater application potential, a similar photoswitching in the solid-state is much less explored. Since Hartley's first report on a spatial rearrangement along the

N=N double bond of azobenzene [5], a plethora of related molecular photoswitches has been developed and it has also been demonstrated that azobenzene can be covalently bound to a photoresponsive polymeric material imparting unique properties. A switchable glass-transition temperature (T_g) and thus resulting self-healing ability is a typical example [6]. As reported by Yu et al. [7], the different T_g of *E* and *Z*-isomers can lead to so called surface photofluidization due to the viscoelastic state of (*Z*)-azobenzene. Hence, the azobenzene-doped polymer can be photo-welded going from the viscoelastic to the glassy state after reverse *Z*→*E* isomerization. Laser-induced surface relief grating (SRG) on azobenzene-containing polymers is another prominent application of the solid-state *E/Z* isomerization [8,9]. Azobenzene was also incorporated into the structure of liquid crystal elastomers (LCEs) [10,11], where UV-light curing increases thermally induced LCE film actuation or even locks the film in a specific shape during flipping [10]. The phenomenon of photoactuation has also been used within the frame of a microgripper constructed from an azobenzene liquid crystal polymer (LCP) [12]. Violet (*E* → *Z*) or green (*Z* → *E*) light can power shapeshifting of this miniature device made of two LCP strips. The photoinduced transition between the heterosmectic and isotropic phase within the liquid crystalline copolymer enables modulation of the proton conductivity, as demonstrated by Nagano et al. [13]. Lin et al. reported on azobenzene-con-

taining peptoids forming hollow spherical supramolecular aggregates (*E*-configuration) that transform into helical arrangement (*Z*-configuration) after irradiation with UV light. Furthermore, when a fluorescent pyrene moiety was embedded into the azopeptoids, the emission wavelength could be significantly modulated via the photoinduced azobenzene *E/Z* switch by allowing Förster resonance energy transfer (FRET) [14]. Azobenzene has also been used to construct a light–heat responsive polyurethane actuator [15], a silicon-based liquid crystalline polyacrylate with photoinduced transition from the smectic mesophase to the isotropic phase [16], a drug delivery system capable to release the drug via *E/Z* isomerization induced by direct (UV) or indirect (NIR) irradiation [17] and epoxyamine glasses with a mechanical softening induced by light [18]. Thermal sensing is another application, which can be addressed using azobenzene-modified polymeric systems (Figure 1). Zou et al. developed a thermal-sensing device based on azobenzene **A** featuring a fluorescence intensity linearly dependent on the temperature [19,20]. Priimagi et al. reported thermal sensors based on the simple azobenzenes **B1–3** by exploiting the dependence of the protonation rate on the temperature, which is accompanied by a color change [21]. Four different azobenzenes **C1–4** were used as liquid crystalline copolymeric pendants in macromolecules capable to change their reflectance with the temperature. This feature potentially enables

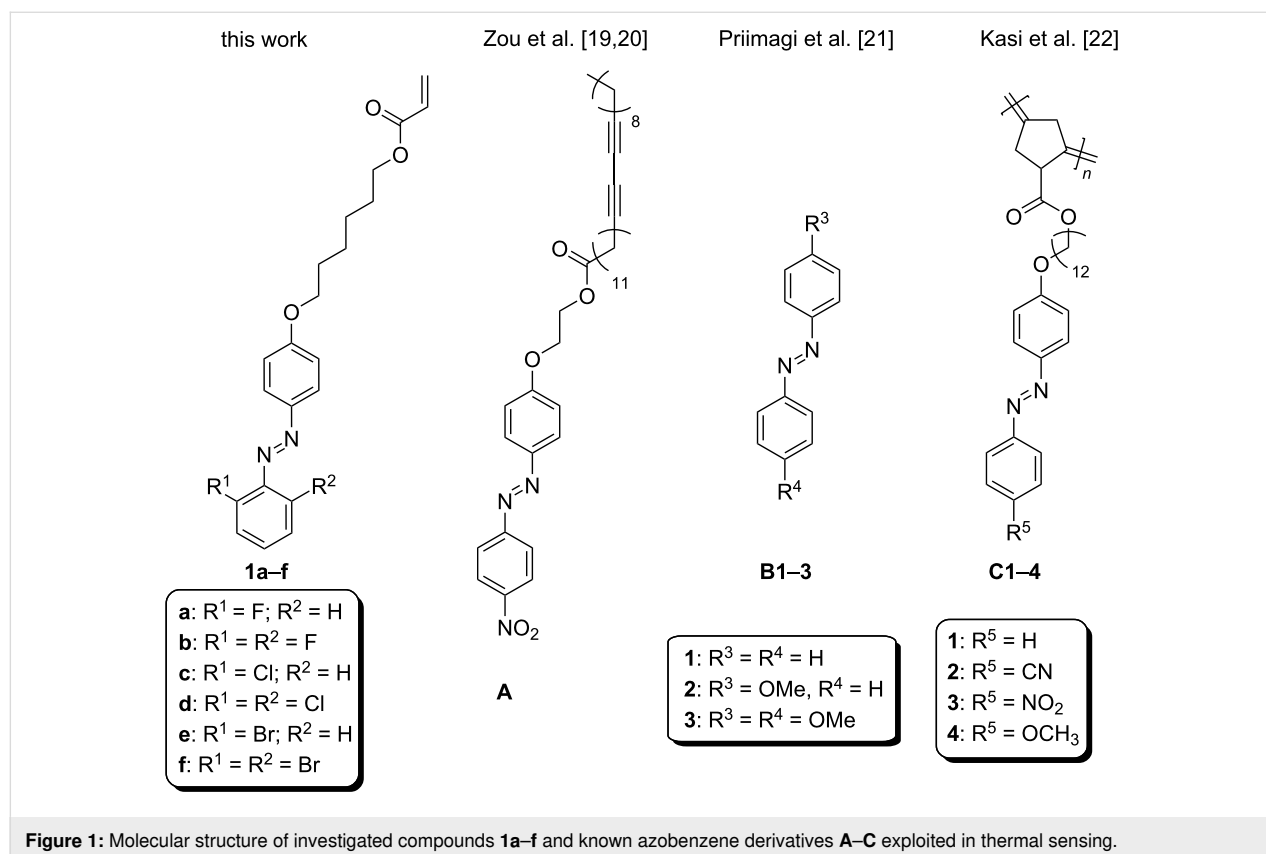


Figure 1: Molecular structure of investigated compounds **1a–f** and known azobenzene derivatives **A–C** exploited in thermal sensing.

their usage in temperature sensing labels [22]. These representative applications clearly demonstrate a wide interest in a light-driven control over the diverse properties of various solid azobenzene polymeric systems.

As an extension of these studies, we report herein a series of six novel azobenzene acrylate monomers **1a–f** (Figure 1) structurally differing in the attached halogen atoms (F, Cl, and Br) at the positions 2 and 6. The described substitution pattern is known to provide a very long half-life of the *Z*-isomer ranging from tens of days to months [23,24]. Photoswitching properties both in solution and in the solid state were investigated along with a potential use of **1a–f** as thermal-sensing labels. For these purposes, differential scanning calorimetry (DSC), thermogravimetric analysis (TGA), cyclic voltammetry (CV), UV–vis absorption spectroscopy, ^1H and ^{13}C NMR, and theoretical DFT calculations were employed. Furthermore, the target compounds are designed for incorporation as photoactive copolymers into the structure of functionalized polyacrylate or polystyrene materials.

Results and Discussion

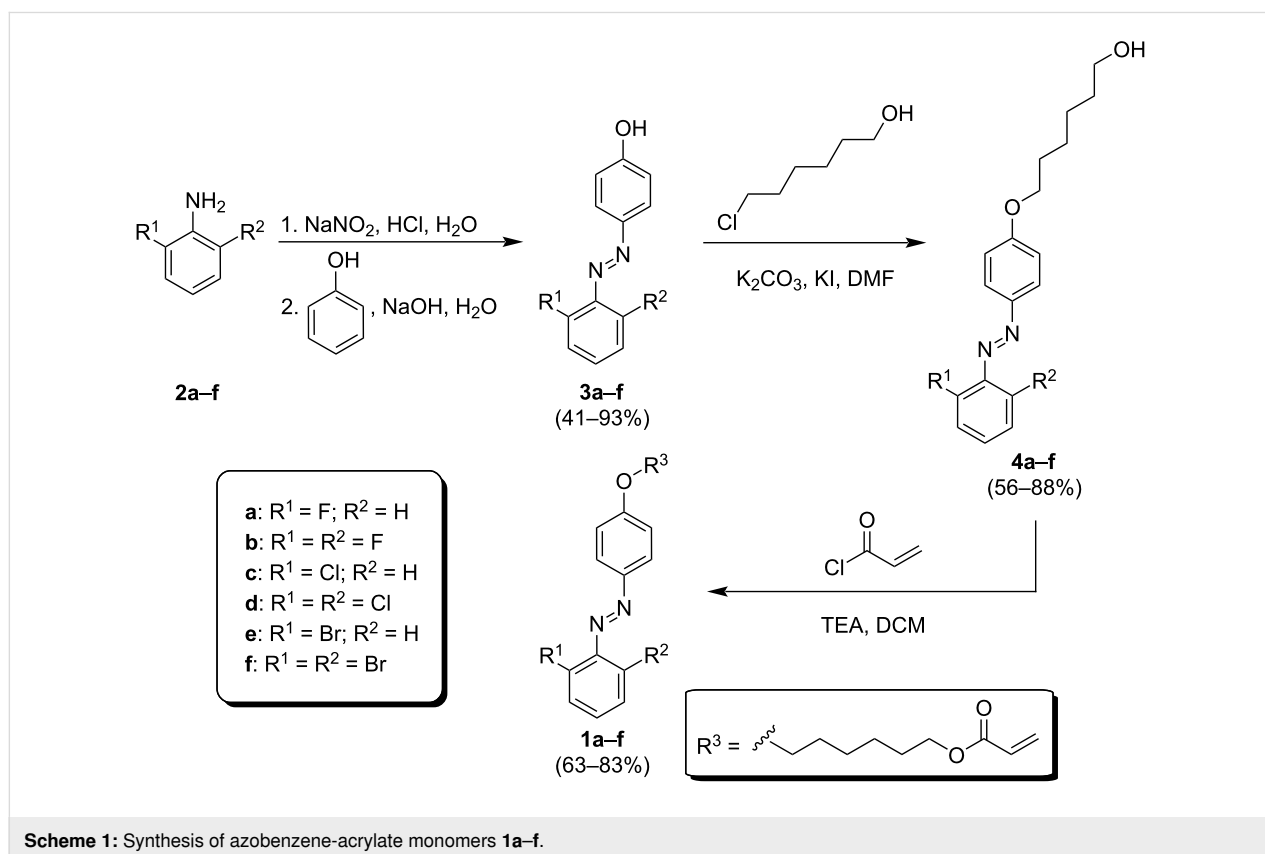
Synthesis of azobenzene monomers

The target azobenzene monomers **1a–f** were obtained using a facile three-step synthetic route as shown in Scheme 1. The first

step represents an azo-coupling reaction between phenol and the corresponding diazonium salts prepared in situ from the commercially available aromatic amines **2a–f** [25]. The reaction was buffered by a 10% aq solution of sodium hydroxide and afforded the azobenzenes **3a–f** with yields ranging from 41 to 93%. These intermediates were further *O*-alkylated using 6-chlorohexanol in the presence of potassium carbonate and potassium iodide to yield alcohols **4a–f** (56–88%) that underwent final acylation with acryloyl chloride [6]. The target azobenzene monomers **1a–f** were prepared with satisfactory yields ranging from 63 to 83%.

Thermal analysis

The thermal behavior of target compounds **1a–f** was investigated by thermogravimetric analysis (TGA) and differential scanning calorimetry (DSC). Based on the TGA measurements, the initial temperature of thermal degradation (T_i) and temperatures of 5% weight loss (T_5) were determined. DSC was used to determine melting points (T_m), glass transition temperatures (T_g), and temperatures of thermal decomposition (T_d). All measured values are summarized in Table 1, while representative thermograms are depicted in Figure 2. Thermograms of all target compounds are listed in Supporting Information File 1, Figures S1–12. The final molecules were isolated as highly viscous liquids or slowly solidified powders, due to the long aliphatic

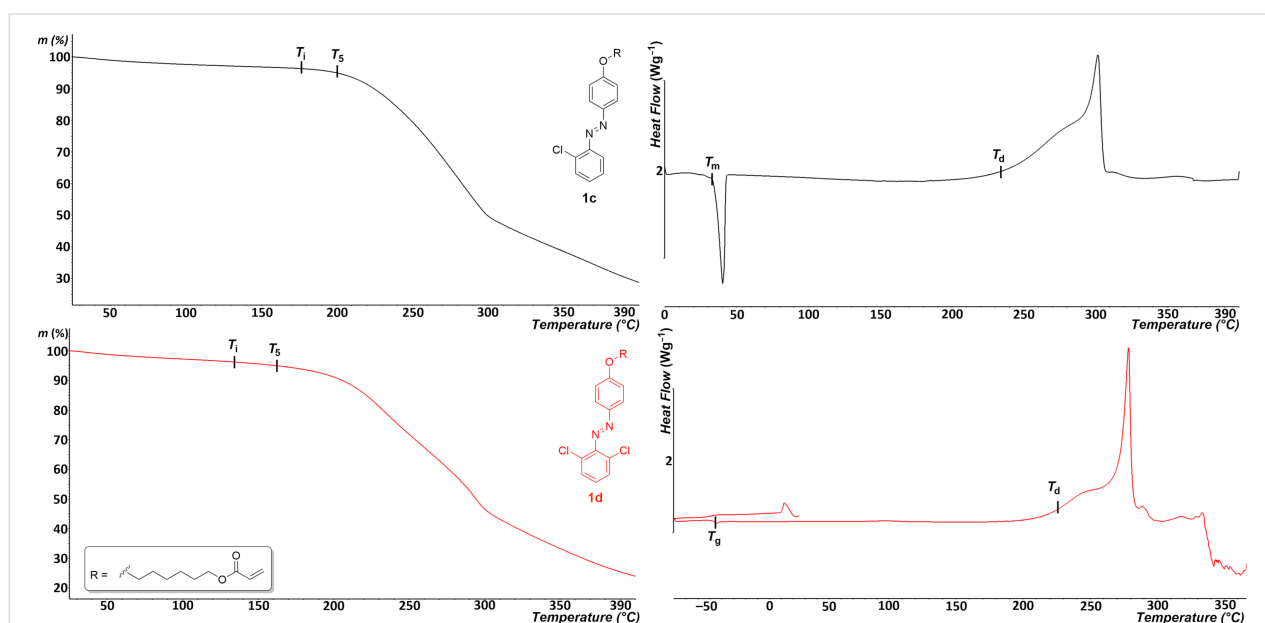


Scheme 1: Synthesis of azobenzene-acrylate monomers **1a–f**.

Table 1: Thermal properties of azobenzenes **1a–f**.

compound	T_i^a [°C]	T_5^a [°C]	T_m^b [°C]	T_g^b [°C]	T_d^b [°C]
1a	175	190	64	–	231
1b	164	209	66	–	236
1c	175	200	33	–	234
1d	134	162	–	–49	229
1e	169	185	–	–45	229
1f	170	195	–	–45	221

^aDetermined by TGA in open alumina crucibles under an N_2 inert atmosphere and with a heating rate of $3\text{ °C}\cdot\text{min}^{-1}$ within the range of $25\text{--}400\text{ °C}$. The initial temperature of thermal degradation was identified as the point where the first derivative of the TGA curve (DTG curve) begins to deviate from its initial plateau. The temperature of 5% weight loss was determined by a gradual horizontal step on the TGA curve. ^bDetermined by DSC in alumina crucibles closed with holed lid under an N_2 inert atmosphere and with a scan rate of $5\text{ °C}\cdot\text{min}^{-1}$ within the range of $0\text{--}400\text{ °C}$ (**1a–c**) or $-80\text{--}400\text{ °C}$ (**1d–f**). The melting points, glass transition temperatures and liquid phase decomposition temperatures were determined as the point of intersection of the baseline and the tangent of the peak (onset point).

**Figure 2:** Representative TGA (left) and DSC (right) curves of compounds **1c** (black) and **1d** (red).

polymerizable pendant, which significantly suppresses facile crystallization. Hence, the target molecules were obtained as semi-crystalline solids undergoing a melting process (**1a–c**) or as viscous liquids (**1d–f**) where only a glass transition occurs upon cooling. This implies that the tendency to crystallize is clearly controlled by the type of the corresponding halide atom(s). When a very small fluorine atom is attached, the planar azobenzene scaffold is most likely to π -stack very efficiently, which is a significant promoter of the crystallization process simultaneously suppressing the counter-effect of the long aliphatic pendant. On the other hand, when a bulky bromine atom is involved, π -stacking is probably much less efficient and only amorphous solidification dominates upon cooling. Whereas the dichloro derivative **1d** is a liquid under normal conditions

(20 °C , 101.325 kPa) with a $T_g = -49\text{ °C}$, monochloro analogue **1c** is a crystalline solid with $T_m = 33\text{ °C}$. From this perspective, the chlorine atom is at the size boundary, thus the number of appended chlorine atoms most likely determines the degree of supramolecular organization, as observed from the different thermal behavior of compounds **1c** and **1d**. The above assumptions clearly follow the experimental data. Hence, an endothermic peak of melting ranging between 33 and 66 °C was clearly determined for molecules **1a–c**, while the viscous liquids **1d–f** solidified only amorphously, which is reflected in the observable glass transitions at around -50 °C . Above the melting points, all molecules were identified as low-volatile liquids that decomposed exothermically upon continued heating. The non-volatile melts of the subseries **1a–c** persist un-

changed until 164–175 °C, where TGA revealed beginning of evaporation, and final decomposition is observed at 231–236 °C as indicated by a broad exothermic peak within the DSC curve. The first weight loss for the viscous liquids **1d–f** was found from 134 to 170 °C (T_i), pointing to a low-volatility of their liquid phase, while the thermal decomposition falls within the range of 221–229 °C. The derivative **1b** bearing the smallest fluorine atoms proved to be the most thermally stable but the differences in T_d values are rather minor. When comparing the T_i values, a slightly higher liquid-phase volatility is seen for the disubstituted analogues (compare **1a** vs **1b**, **1c** vs **1d**; except for the bromine derivatives **1e** and **1f** where T_i is almost equal). The most pronounced difference was recorded for the chloro-substituted pair **1c** and **1d** ($\Delta T_i = 41$ °C).

Electrochemistry

The electrochemical behavior of azo-compounds **1a–f** was investigated in 1,2-dichloroethane (DCE) containing 0.1 M Bu_4NPF_6 in a three-electrode cell by cyclic voltammetry (CV). The recorded peak potentials are given vs Ag/AgCl reference electrode (SSCE). The acquired electrochemical data obtained in DCE are summarized in Table 2 including DFT-calculated values while the corresponding HOMO/LUMO levels are visualized in Figure 3. Further experimental details and particular CV diagrams are given in Supporting Information File 1, Figures S13–18.

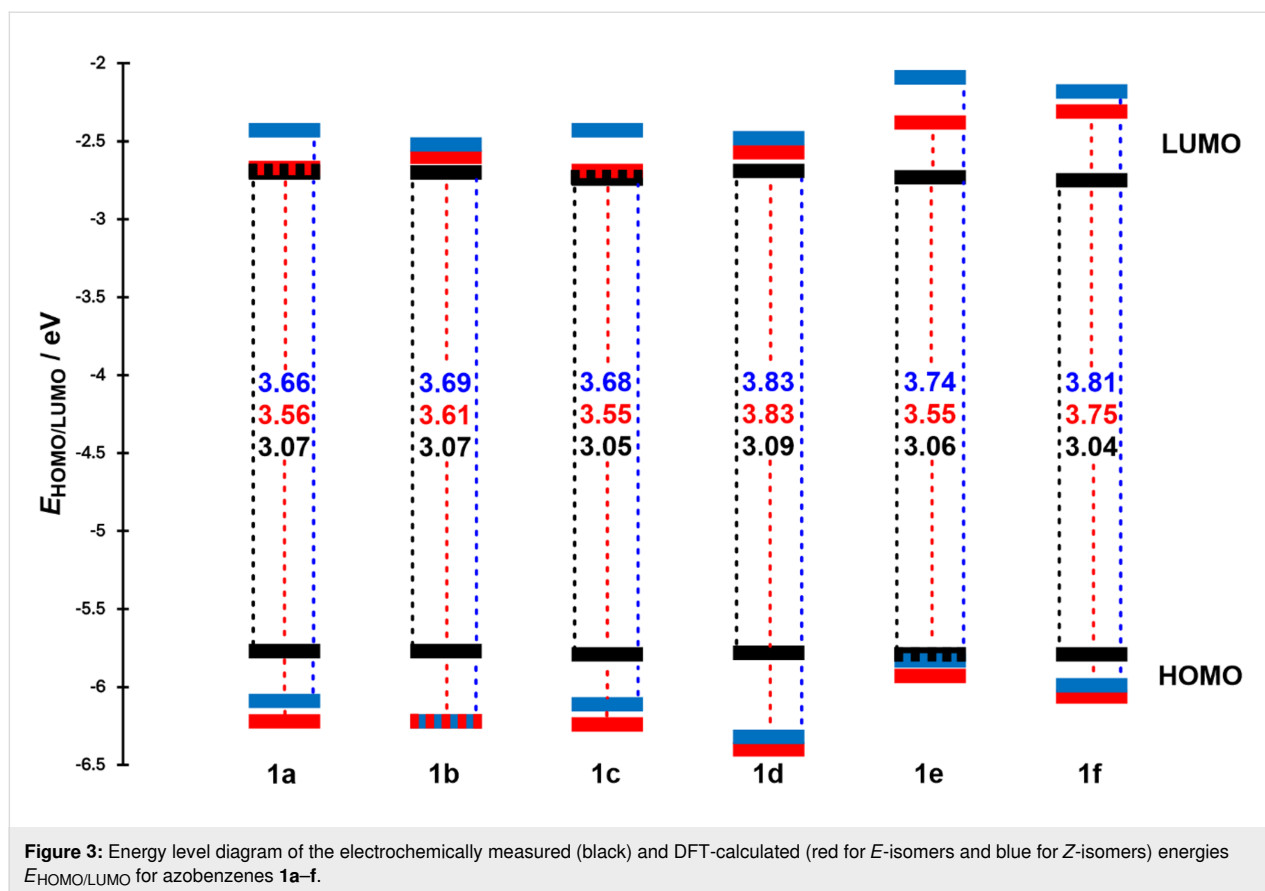
Compounds **1a–f** exhibited very similar electrochemical features reflecting their analogous structures, which differ only in the type and the number of appended halogens. One reduction and one oxidation processes were found within the available potential window of DCE. Both electrochemical redox processes are irreversible regardless the scan rate, indicating chemical instability of the generated oxidized/reduced forms in the

used system. The reverse reduction of the chemically modified oxidized form was recorded as a broad peak at significant undervoltage, especially for derivatives **1a–b** and **1d–e**. The electrochemical data suggest that the first oxidation and the first reduction processes are associated with different parts of the molecule. Considering the structural features and the measured peak potentials $E_p^{\text{red1,cat}}$ around -1.6 V, the first reduction process is most reasonably assigned to the azo group, since azobenzene and related azo-derivatives are known to undergo an initial one-electron reduction at the N=N bond, affording the corresponding radical anion [27]. In contrast, possible reduction of an aliphatic ester substituent, such as our acrylate pendant, generally requires more negative potentials [28]. On the other hand, the first oxidation observed at ca. $+1.47$ V is most likely associated with the alkoxy donor fragment, in agreement with literature data showing that anisole- and methoxy-arene-type systems typically undergo an initial oxidation of the alkoxyaryl unit [29–31]. In addition, possible oxidation involving the aryl halide moiety generally requires a more positive potential [28]. Taken together, these data support the assignment of the first oxidation to the alkoxy donor moiety and the first reduction to the azobenzene acceptor fragment. If we consider the reduction of the azo bond as a one-electron process, a mutual comparison of the current maxima of the first oxidation and reduction provided an approximate ratio of $i_p^{\text{red1,cat}}$ vs $i_p^{\text{ox1,an}} = 1:3$ for compounds **1a–e**. This indicates a three-electron process within the first oxidation, implying parallel oxidation of the “phenolic” oxygen and the adjacent π -system. The mutual ratio of both current maxima was more balanced in the case of the dibromo analogue **1f**, indicating an oxidation of the phenolic moiety is more difficult. As summarized in Table 2 and visualized in the energy level diagram (Figure 3), the electrochemical measurements point to the steady HOMO and LUMO energies and their differences

Table 2: The electrochemically measured and DFT-calculated data of target azobenzenes **1a–f**.

compd.	$E_p^{\text{ox1,an}}$ [V] ^a	$E_p^{\text{red1,cat}}$ [V] ^b	E_{HOMO} [eV] ^c	E_{LUMO} [eV] ^d	ΔE [eV] ^e	E_{HOMO} DFT (E) [eV]	E_{LUMO} DFT (E) [eV]	ΔE DFT (E) [eV]	E_{HOMO} DFT (Z) [eV]	E_{LUMO} DFT (Z) [eV]	ΔE DFT (Z) [eV]
1a	1.46	-1.61	-5.77	-2.70	3.07	-6.22 ^f	-2.67 ^f	3.56	-6.09 ^f	-2.43 ^f	3.66
1b	1.46	-1.61	-5.77	-2.70	3.07	-6.22 ^f	-2.60 ^f	3.61	-6.22 ^f	-2.52 ^f	3.69
1c	1.48	-1.57	-5.79	-2.74	3.05	-6.24 ^f	-2.69 ^f	3.55	-6.11 ^f	-2.43 ^f	3.68
1d	1.47	-1.62	-5.78	-2.69	3.09	-6.40 ^f	-2.57 ^f	3.83	-6.32 ^f	-2.48 ^f	3.83
1e	1.48	-1.58	-5.79	-2.73	3.06	-5.93 ^g	-2.38 ^g	3.55	-5.83 ^g	-2.09 ^g	3.74
1f	1.48	-1.56	-5.79	-2.75	3.04	-6.06 ^g	-2.31 ^g	3.75	-5.99 ^g	-2.18 ^g	3.81

^a $E_p^{\text{ox1,an}}$ is the anodic peak potential of the irreversible first oxidation process. ^b $E_p^{\text{red1,cat}}$ is the cathodic peak potential of the irreversible first reduction process. $E_p^{\text{ox1,an}}$ and $E_p^{\text{red1,cat}}$ were measured by CV in DCE containing 0.1 M Bu_4NPF_6 ; all potentials are given vs Ag/AgCl reference electrode ($+0.205$ V vs SHE). ^c $E_{\text{HOMO}} = -(E_p^{\text{ox1,an}} - 0.49 + 4.8)$ [26]. ^d $E_{\text{LUMO}} = -(E_p^{\text{red1,cat}} - 0.49 + 4.8)$ [26]. ^e $\Delta E = E_p^{\text{ox1,an}} - E_p^{\text{red1,cat}}$. ^fCalculated at the B3LYP 6-311+g(2d,p) level of theory in DCE. ^gCalculated at the B3LYP 6-31g(d) level of theory in DCE.



$\Delta E = 3.05\text{--}3.09$ eV. The experimental data are corroborated by DFT results calculated for both isomers (Table 2). The highest HOMO–LUMO gap was measured/calculated for the dichloro derivative **1d**, while the monosubstituted ones (**1a**, **c** and **e**) possess the narrowest ΔE values. As expected, the calculations further indicate the lower HOMO/LUMO energies/gaps for the *E*-isomers as compared to the *Z*-isomers.

Linear optical properties

Fundamental optical properties of the target azobenzenes **1a–f** in solution were investigated by electronic absorption spectra at 20 °C in DCE at a concentration of 4×10^{-5} M. The absorption maxima for both isomers ($\lambda_{\text{max}}^{E/Z}$) and the corresponding molar absorption coefficients ($\epsilon^{E/Z}$) along with the TD-DFT calculated absorption maxima ($\lambda_{\text{max}}^{E/Z}$ (CAM-)B3LYP) are summarized in Table 3. Representative spectra of compounds **1a**, **c** and **e** corresponding to their dark-adapted photostationary state (PSS; pure *E*-isomers) are shown in Figure 4A, while the calculated spectra of the pure *Z*-isomers are depicted in Figure 4B. Complete listing of all UV–vis absorption spectra can be found in Supporting Information File 1, Figures S19–23. The spectra of the pure *Z*-isomers were calculated using the method by Fischer [32]. Whereas Figure 4 demonstrates a minor effect of the different halogen atoms, attaching a second halogen atom

(e.g., mono/dichloro derivatives **1c** and **1d** in Figure 5) has more pronounced effect (red-shift). The shape of the obtained spectra is as expected for azobenzene derivatives with the *E*-isomers featuring a dominant band appearing at 270–400 nm (the $\pi\text{--}\pi^*$ electronic transition) accompanied by a weak band at 400–510 nm (the $n\text{--}\pi^*$ electronic transition). The absorption spectra of the *Z*-isomers comprise a blue-shifted $\pi\text{--}\pi^*$ band (250–350 nm) with a diminished molar absorption coefficient and a slightly pronounced $n\text{--}\pi^*$ band (350–530 nm).

An angle between both benzene ring planes denoted as $\phi_{E/Z}$ has been employed to judge planarity of both isomers (see Supporting Information File 1, Table S1). The monosubstituted *E*-isomers are nearly planar ($\phi_E = 168\text{--}180^\circ$), while the disubstituted *E*-isomers are rather twisted with $\phi_E = 122\text{--}146^\circ$. The nonplanar arrangement of the latter results in a diminished extent of conjugation, which accounts for the blue-shifted maxima (λ_{max}^E of **1b**, **d** and **f** in Table 3). On the contrary, the differences in λ_{max}^Z are rather minor (see Supporting Information File 1, Table S1 for ϕ_Z) but the longest-wavelength absorption maxima of the disubstituted *Z*-isomers are red-shifted by ≈ 5 nm. Considering very similar ϕ_Z values for all three investigated pairs, λ_{max}^Z is influenced rather electronically via the second halogen atom.

Table 3: Experimentally measured and theoretically calculated optical properties of azobenzenes **1a–f**.

compd.	λ_{max}^E [nm (eV)] ^a	ϵ^E [$\times 10^3 \text{ M}^{-1} \text{ cm}^{-1}$] ^a	λ_{max}^Z [nm (eV)] ^b	ϵ^Z [$\times 10^3 \text{ M}^{-1} \text{ cm}^{-1}$] ^b	λ_{max}^E (B3LYP) [nm (eV)]	λ_{max}^Z (B3LYP) [nm (eV)]	λ_{max}^E (CAM-B3LYP) [nm (eV)]	λ_{max}^Z (CAM-B3LYP) [nm (eV)]
1a	355 (3.49)	15.8	312 (3.97)	7.1	386 (3.21) ^c	331 (3.75) ^c	351 (3.53) ^d	294 (4.22) ^d
1b	343 (3.62)	16.9	317 (3.91)	7.8	369 (3.36) ^c	329 (3.77) ^c	338 (3.67) ^d	295 (4.20) ^d
1c	360 (3.44)	15.7	312 (3.97)	8.9	388 (3.20) ^c	328 (3.78) ^c	351 (3.53) ^d	292 (4.25) ^d
1d	333 (3.72)	18.0	317 (3.91)	7.0	348 (3.56) ^c	323 (3.84) ^c	316 (3.92) ^d	292 (4.25) ^d
1e	360 (3.44)	17.4	312 (3.97)	7.8	384 (3.23) ^e	328 (3.78) ^e	347 (3.57) ^f	289 (4.29) ^f
1f	333 (3.72)	19.3	318 (3.90)	8.8	353 (3.51) ^e	334 (3.71) ^e	319 (3.89) ^f	294 (4.22) ^f

^aMeasured in DCE at a concentration of 4×10^{-5} M for the dark-adapted PSS. ^bDetermined from the calculated spectra of pure *Z*-isomer. ^cCalculated at the B3LYP 6-311++g(2d,p) level of theory in DCE. ^dCalculated at the CAM-B3LYP 6-311++g(2d,p) level of theory in DCE. ^eCalculated at the B3LYP 6-31g(d) level of theory in DCE. ^fCalculated at the CAM-B3LYP 6-31g(d) level of theory in DCE.

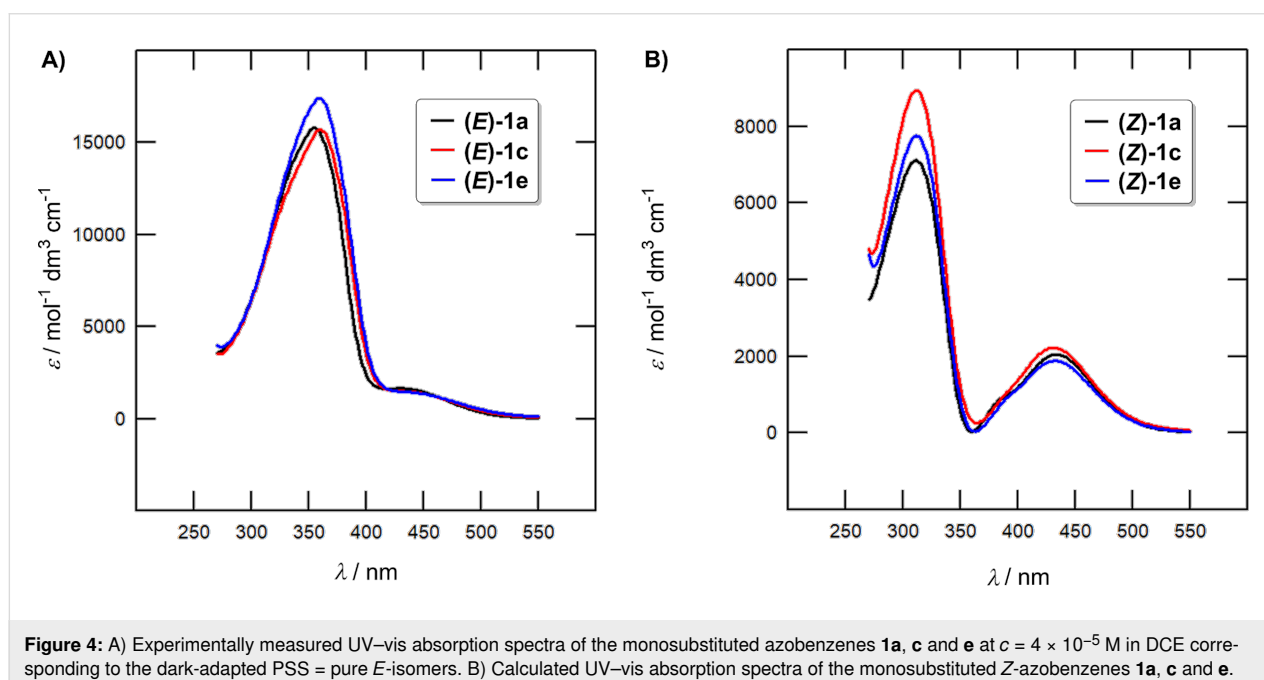
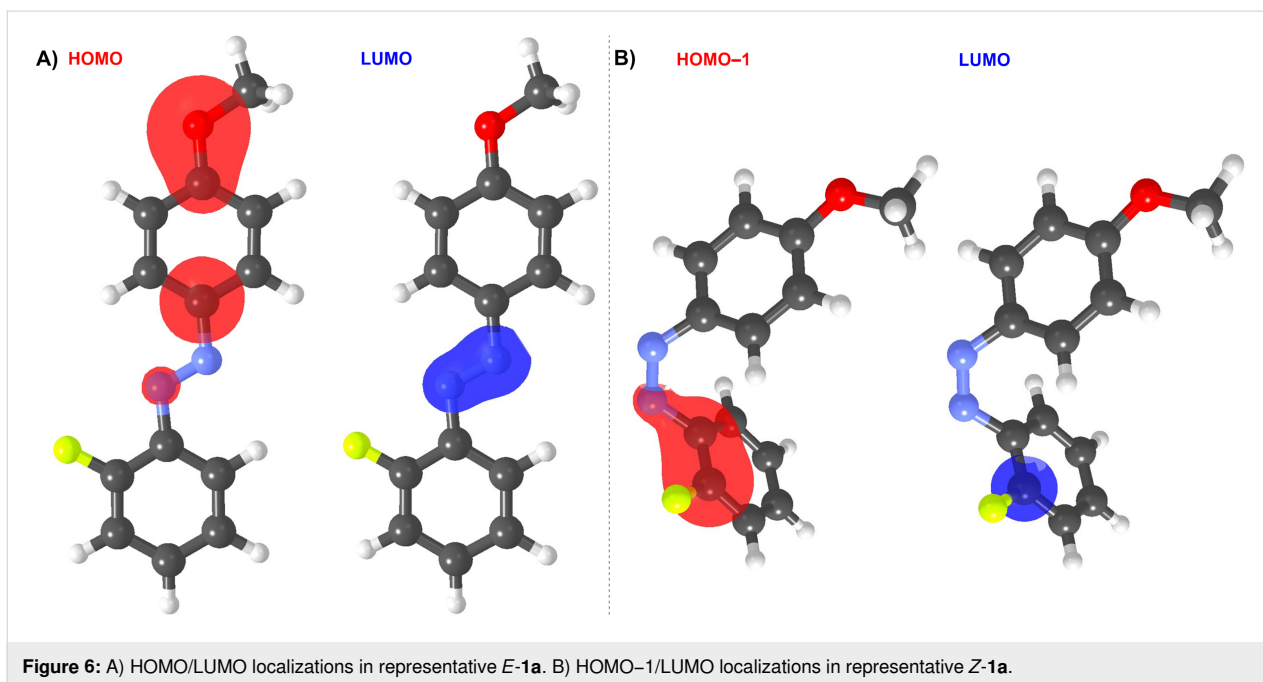
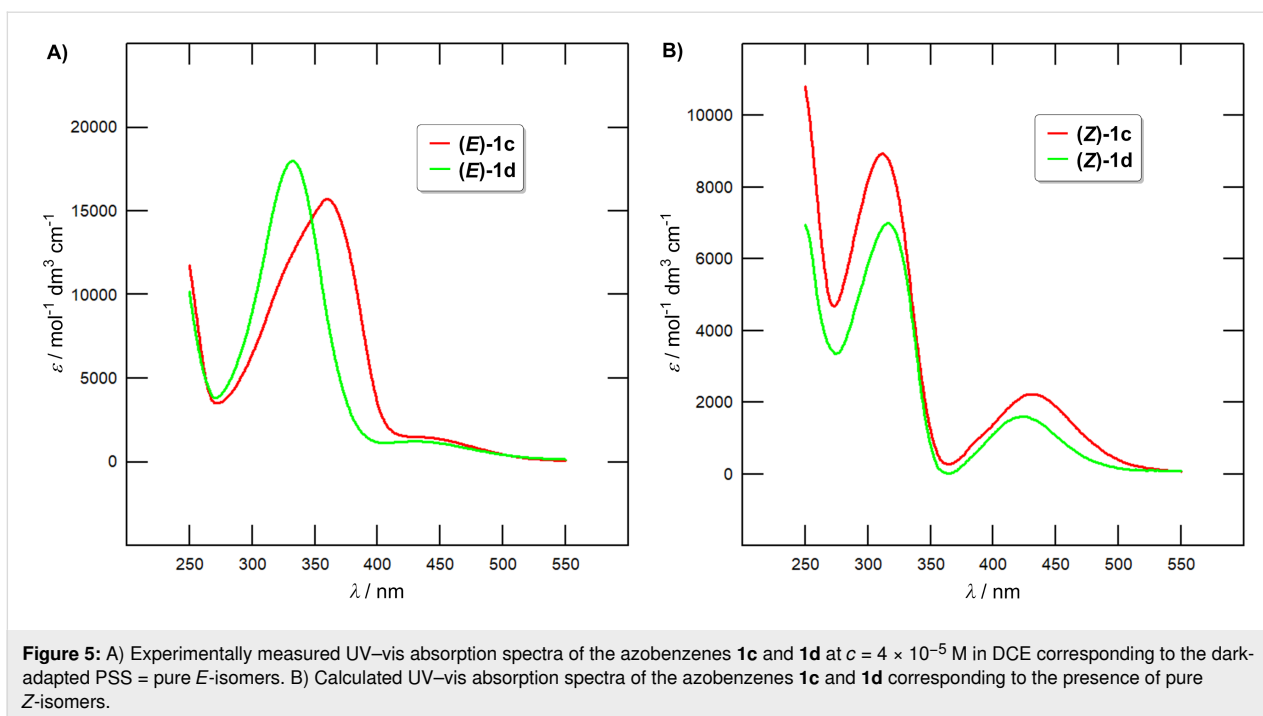


Figure 4: A) Experimentally measured UV–vis absorption spectra of the monosubstituted azobenzenes **1a**, **c** and **e** at $c = 4 \times 10^{-5}$ M in DCE corresponding to the dark-adapted PSS = pure *E*-isomers. B) Calculated UV–vis absorption spectra of the monosubstituted *Z*-azobenzenes **1a**, **c** and **e**.

The UV–vis absorption spectra were further predicted via TD-DFT and using B3LYP and CAM-B3LYP functionals (Table 3 and Supporting Information File 1, Figures S65–88). Both methods afforded the spectra that are similar in shape but either red or blue-shifted compared to the experimental data. The range-separated CAM-B3LYP functional was used to better describe the excited states and charge-transfer character of the investigated molecules. Anyway, both methods confirmed a minor effect of the halogen type, red-shifted λ_{max}^E values for monosubstituted *E*-isomers and the opposite trend for

the *Z*-isomers. TD-DFT calculations revealed the most intense absorption bands of (*E*)- and (*Z*)-azobenzenes are generated by HOMO→LUMO or HOMO–1→LUMO transitions, respectively. The involved orbitals visualized in Figure 6 reveal the phenol-centered HOMO and the azo-linker occupied by the LUMO in (*E*)-**1a**, while in (*Z*)-**1a** both HOMO–1 and LUMO are spread over the fluorophenyl moiety (ditto for the disubstituted derivatives). See Supporting Information File 1, Figures S53–64 for a similar visualization of the frontier molecular orbitals in all studied molecules.



Photoinduced *E/Z*-isomerization

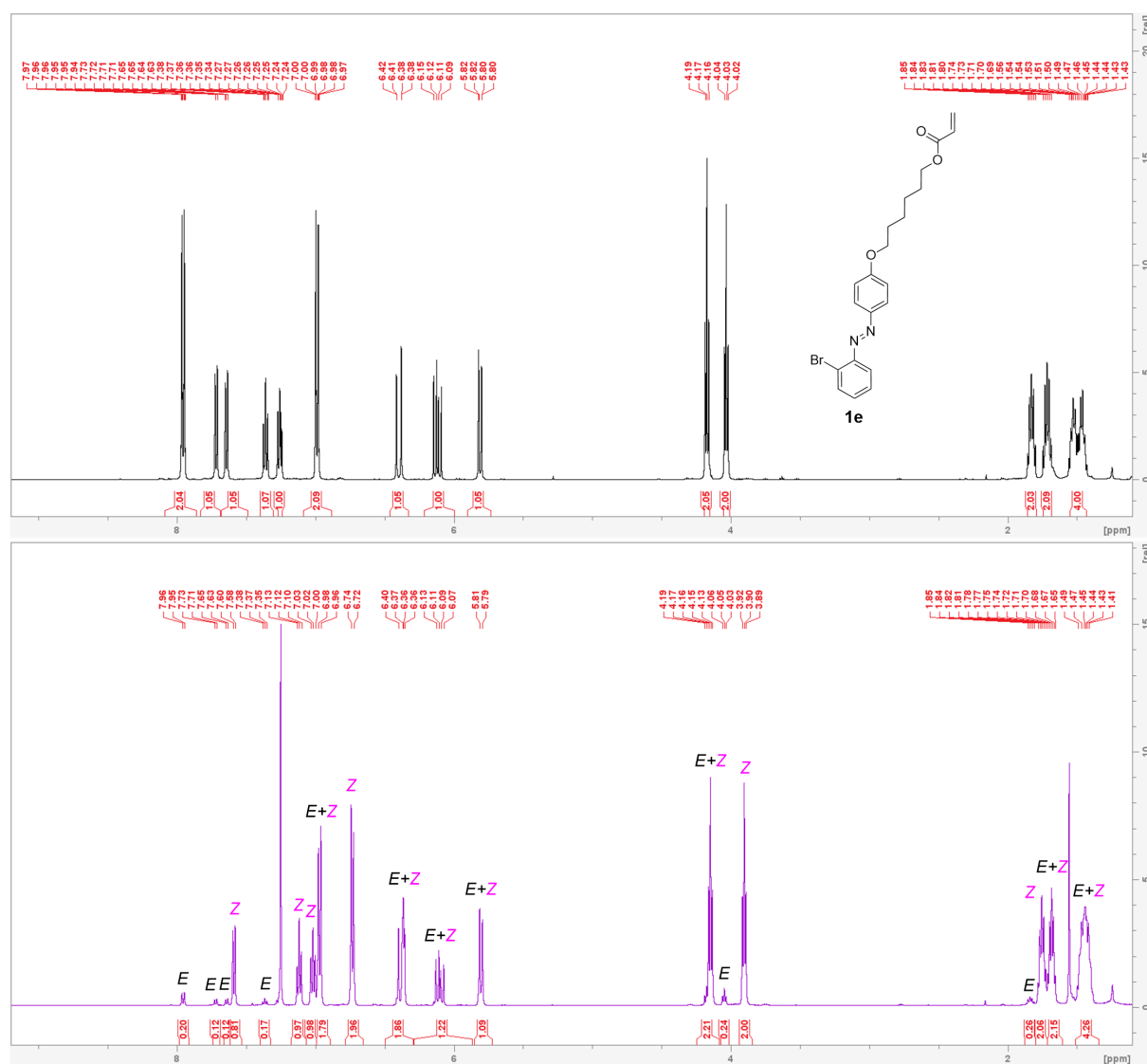
The photoinduced $E \leftrightarrow Z$ switching was investigated using 355 nm (forward switch) and 430 nm (reverse switch) LEDs. The *E/Z* molar ratios corresponding to the appropriate photostationary state (PSS), the half-lives of the *Z*-isomer in the dark ($\tau_{1/2}$) and the rate constants of the thermal relaxation in the dark (k) were determined by UV–vis absorption and ^1H NMR spectroscopies and are summarized in Table 4. Due to very

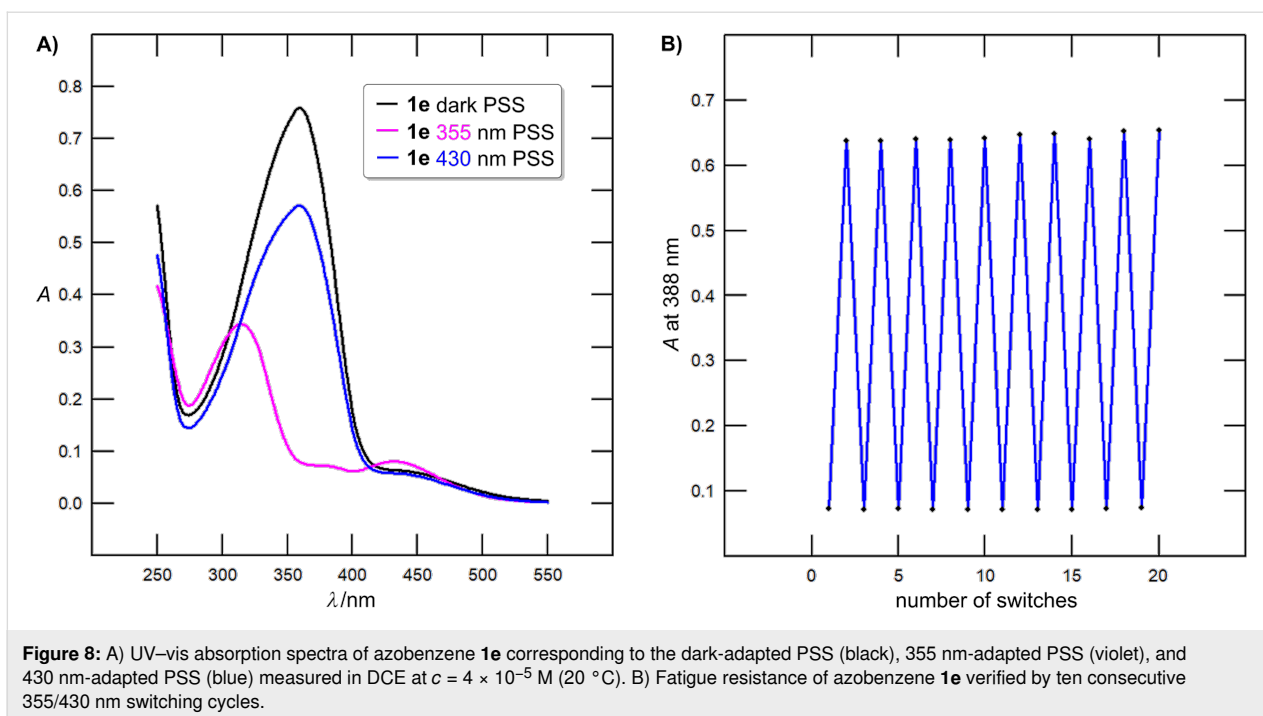
slow thermal $Z \rightarrow E$ relaxation at laboratory temperature (20 °C), the $\tau_{1/2}$ and k were measured at 60 °C. The method for its determination is described in our previous article [3]. Figure 7 compares the ^1H NMR spectra of the dark-adapted and 355 nm-adapted photostationary states of compound **1e**, while Figure 8 show an analogous comparison using UV–vis absorption spectra along with a fatigue resistance verification. Representative thermal kinetic curves obtained by both UV–vis

Table 4: The *E/Z* molar ratios, the *Z*-isomer half-lives and the rate constants of azobenzenes **1a–f** determined from the UV–vis and NMR spectra.

compd.	<i>E/Z</i> fwd. switch (UV–vis) ^{a,b}	<i>E/Z</i> rev. switch (UV–vis) ^{a,c}	$\tau_{1/2}$ (UV–vis) [h] ^a	<i>k</i> (UV–vis) [s ⁻¹] ^a	<i>E/Z</i> fwd. switch (NMR) ^{b,d}	$\tau_{1/2}$ (NMR) [h] ^d	<i>k</i> (NMR) [s ⁻¹] ^d
1a	7:93	77:23	1.50	1.3×10^{-4}	9:91	1.82	1.1×10^{-4}
1b	15:85	82:18	3.74	5.1×10^{-5}	54:46	6.59	2.9×10^{-5}
1c	8:92	92:8	1.23	1.6×10^{-4}	77:23	1.43	1.3×10^{-4}
1d	33:67	79:21	2.21	8.7×10^{-5}	41:59	1.79	1.1×10^{-4}
1e	7:93	73:27	1.61	1.2×10^{-4}	11:89	1.82	1.1×10^{-4}
1f	36:64	82:18	1.27	1.5×10^{-4}	28:72	1.72	1.1×10^{-4}

^aDetermined from the UV–vis absorption spectra measured at 20 °C in DCE at $c = 4 \times 10^{-5}$ M; (fwd. = forward, rev. = reverse). ^bDetermined at the 355 nm-adapted PSS. ^cDetermined at the 430 nm-adapted PSS. ^dDetermined from ¹H NMR spectra measured at 20 °C in CDCl₃ at $c = 1 \times 10^{-2}$ M.

**Figure 7:** ¹H NMR spectra (500 MHz, CDCl₃, 20 °C) of azobenzene **1e** corresponding to the dark-adapted PSS (black) and 355 nm-adapted PSS (violet).



absorption and ^1H NMR spectroscopy are shown in Figure 9. Thermal kinetics were optimized using the OPstat 6.10 software [33]. See Supporting Information File 1 for a complete list of analogous figures for all target azobenzenes **1a–f** (Figures S24–35, S39–50, and S89–94). The DFT-calculated E/Z isomerization energies ($\Delta G_{E/Z}$) as a dependence of the substitution

(Table S1 and Figure S52, Supporting Information File 1) indicates that ΔG_E decreases when increasing the size and the number of the appended halogen(s) ($\text{F} > \text{Cl} > \text{Br}$). Similarly, the calculated dipole moment of the E -isomers (μ_E) increases with increasing the atomic radius (r) of the attached halogen ($\text{F} < \text{Cl} < \text{Br}$) for both mono- and disubstituted E -isomers

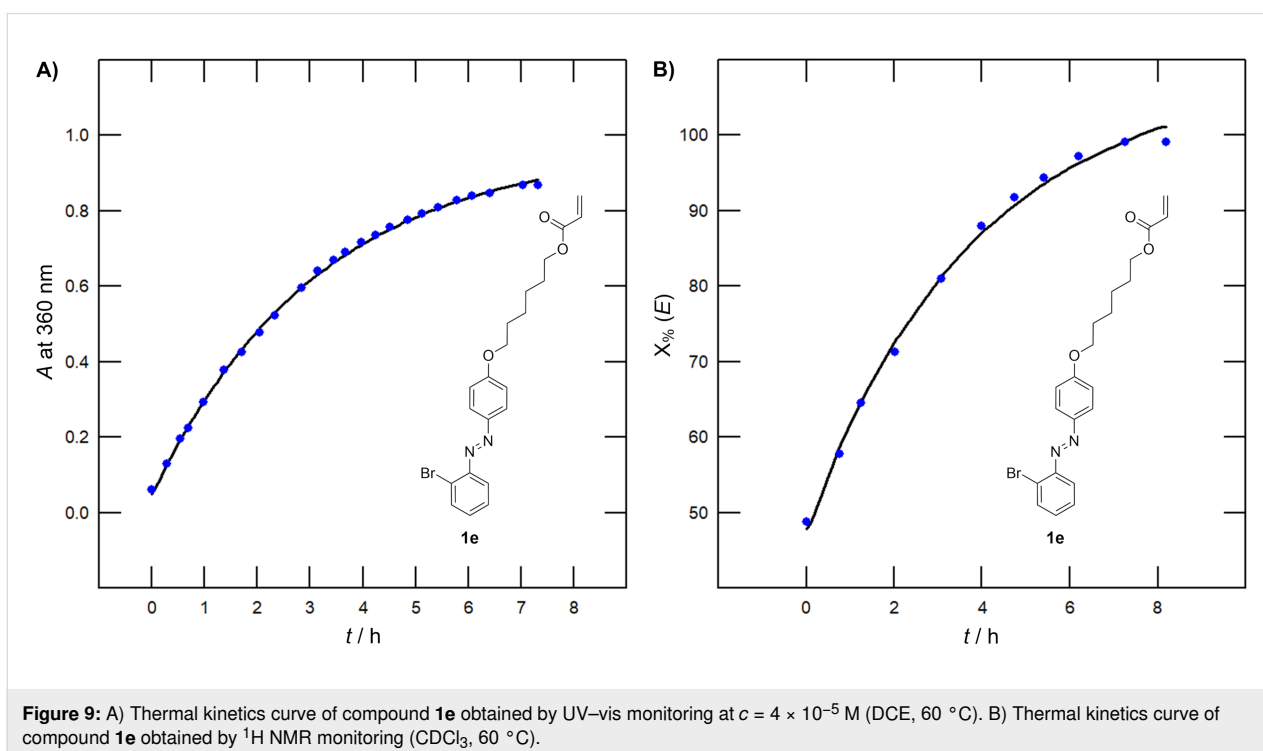


(Table S1 and Figure S52, Supporting Information File 1); the disubstituted *E*-isomers always possess lower μ_E values. These trends are not obeyed for *Z*-isomers where $\mu_Z > \mu_E$.

The *E* → *Z* photoconversion induced by 355 nm light monitored by UV–vis spectroscopy revealed monohalogenated compounds **1a**, **c** and **e** (*E/Z* = 8:92–7:93, Table 4) as the most efficient photoswitches. In general, all monohalogenated switches reached higher photoconversion by ≈20% as compared to dihalogen-substituted ones. However, it should be noted that the absorption maxima of dihalogenated switches are blue-shifted and, provided a short-wavelength LED will be used, the photoconversion could be higher. The type of halogen has only a negligible effect. The reverse switch of **1a–f** induced by 430 nm light afforded the *E/Z* molar ratios of 73:27–92:8 with no straightforward structure–switching property relationships. The recorded half-lives of the *Z*-isomer in the dark ($\tau_{1/2}$) range from 1.23 to 3.74 hours at 60 °C with the largest values recorded for the difluoro/chloro derivatives **1b** and **1d**.

Monitoring of the photoswitching was further carried out using ^1H NMR spectroscopy in CDCl_3 and $c = 1 \times 10^{-2}$ M (slightly different conditions than those used for UV–vis spectroscopy (DCE and $c = 4 \times 10^{-5}$ M) which can influence the obtained kinetic parameters). These measurements confirmed similar effects of adding the second halogen, with the highest *E* → *Z* photoconversion seen for the monosubstituted switches and also the trends seen for $\tau_{1/2}$ values. The latter is further demonstrated by correlating $\tau_{1/2}$ differences between the mono- and

dihalogen analogues (e.g., **1a** vs **1b**) obtained by UV–vis absorption and ^1H NMR spectroscopies (see Supporting Information File 1, Figure S36), while Figure S37 correlates the decreasing $\tau_{1/2}$ values ($\text{F} > \text{Cl} > \text{Br}$) within the dihalogen subseries. Compared to the UV–vis investigation, all azobenzenes possess higher $\tau_{1/2}$ determined by ^1H NMR (Supporting Information File 1, Figure S38); the difluoro derivative **1b** ($\tau_{1/2} = 3.74/6.59$ h (UV–vis/NMR)) possesses the most thermally stable *Z*-isomer. The monochloro compound **1c** showed only poor 355 nm-induced conversion (*E/Z* = 77:23), which contrasts the value found by UV–vis measurement (*E/Z* = 8:92). The fatigue resistance of compounds **1a–f** (Figure 8B) was verified by ten consecutive 355/430 nm switching cycles revealing no structural degradation and photobleaching.

Azobenzene monomers **1a–f** were further incorporated into a thin polystyrene film to study their behavior in the solid state at various concentrations (see the Supporting Information File 1 for a detailed procedure). Judging by naked eye, the *E* → *Z* photoswitch was clearly evident using monofluoro derivative **1a** (Figure 10A–D). The original pale-yellow color changed into dark yellow upon irradiation with 355 nm LED (Figure 10A) reflecting the *E* → *Z* switch. The irradiated sample was kept in the dark at 22 °C and the magnitude of color change was visually verified after 20, 40, and 90 days as shown in Figure 10B–D. Even after 90 days in the dark, high color saturation was still noticeable. The eventual thermal back *Z* → *E* switching was investigated in the dark at 60 °C during 14 h revealing a minor change in the shade and pointing to a high

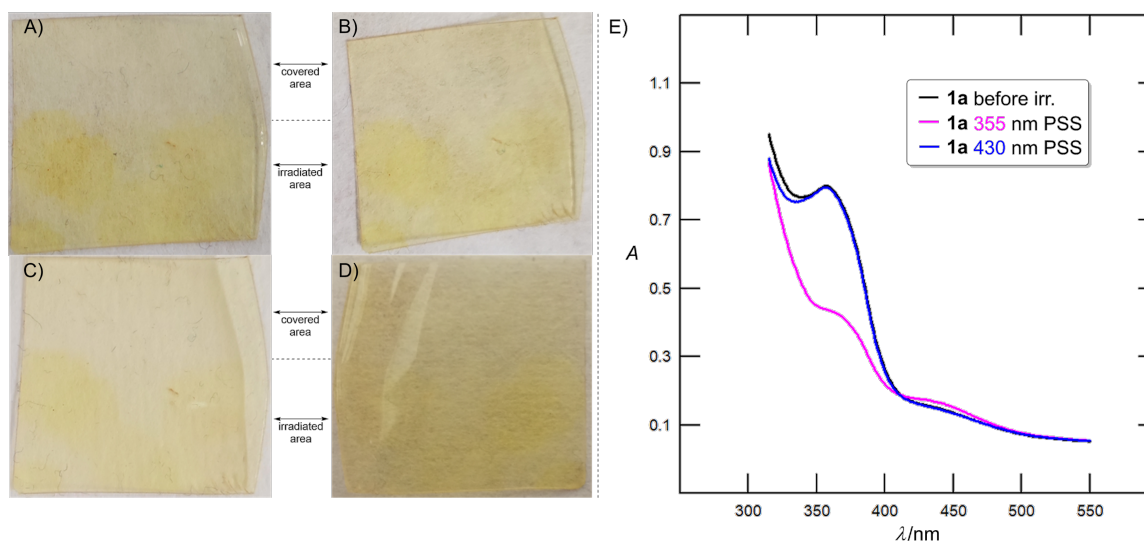


Figure 10: Photoswitching of target azobenzene **1a** in the solid state (polymeric matrix). A) Polystyrene thin film partly irradiated with 355 nm for 2 hours. B) Polystyrene thin film partly irradiated with 355 nm after 20 days in the dark at 22 °C. C) Polystyrene thin film partly irradiated with 355 nm after 40 days in the dark at 22 °C. D) Polystyrene thin film partly irradiated with 355 nm after 90 days in the dark at 22 °C. E) UV–vis absorption spectra of the acrylate thin film corresponding to the state before irradiation (black), 355 nm-adapted PSS (violet, 10 min of irradiation), and 430 nm-adapted PSS (blue, 30 min of irradiation) measured at 20 °C.

thermal stability of **Z-1a** in the polystyrene film. Azobenzene **1a** was also copolymerized with an acrylate matrix. The photo-switching performance of the resulting film (Figure 10E) includes a 355 nm-induced $E \rightarrow Z$ switch with a minimal rate of 55% and the 430 nm-induced reverse $Z \rightarrow E$ switch fully regenerating the E -isomer.

Conclusion

In summary, six novel azobenzene acrylate monomers **1a–f** bearing one or two additional F, Cl and Br atoms were designed and prepared in a straightforward three-step synthesis. Their fundamental properties were investigated in solution and polymeric matrix. TGA and DSC studies revealed different thermal behavior of mono- and disubstituted derivatives, which most likely results from their (non)planar arrangement as supported by DFT results. The electrochemical differences are rather minor, and the type and the number of the appended halogens do not play a significant role. However, the optical properties and particularly the forward $E \rightarrow Z$ switch induced by 355 nm light, depends on the substitution pattern. Monohalogen derivatives **1a**, **1c**, and **1e** exhibited superior photo-switching in solution, reaching the Z -isomer with 92–93% efficiency. In contrast, dihalogen analogues showed $\approx 20\%$ lower efficiency of the photoconversion rate. It has been shown that planarity of the E -isomers depends on the substitution. While monohalogen derivatives are planar, nonplanar disubstituted derivatives with diminished conjugation possess blue-shifted absorption and lower conversion efficiency. The stability of the resulting Z -isomers ($\tau_{1/2}$ values) can be tuned similarly. In solution, the difluoro derivative **1b** was identified as the most stable and efficient photoswitch with the longest half-life of the Z -isomer ($\tau_{1/2} = 3.74$ h at 60 °C in DCE and 6.59 h at 60 °C in CDCl_3). However, copolymerization of **1a–f** with styrene revealed that only the monofluoro-substituted azobenzene **1a** forms a photoresponsive system with a macroscopically visible color change upon irradiation that persisted in the dark at 22 °C for over 90 days. This remarkable stability in a polymeric environment highlights the facile halogen substitution at the positions 2 and 6 as a powerful tool to tune photoswitching performance and the potential of these materials for long-term utilization as molecular photoswitches.

Supporting Information

Supporting Information File 1

Experimental section, characterization data and details on compound analyses.

[<https://www.beilstein-journals.org/bjoc/content/supplementary/1860-5397-22-60-S1.pdf>]

Funding

The work was supported by the Technology Agency of the Czech Republic, Sigma (project No. TQ03000624 “Photoreponsive azo-polymeric materials applied as a thermal sensor”).

Author Contributions

Martina Vachtlová: investigation; methodology; visualization; writing – original draft. Michaela Fecková: conceptualization; investigation; methodology; project administration. Vítězslav Zima: conceptualization; funding acquisition; investigation; methodology; project administration. Jan Podlesný: conceptualization; formal analysis; funding acquisition; investigation; methodology; project administration; validation; visualization; writing – original draft. Milan Klikar: formal analysis; investigation; methodology; visualization; writing – original draft. Oldřich Pytela: formal analysis; software. Patrik Pařík: investigation. Jakub Opršal: investigation; methodology. Eliška Juhaňáková: investigation. Veronika Chrtová: investigation. Filip Bureš: conceptualization; funding acquisition; project administration; supervision; writing – original draft.

ORCID® iDs

Martina Vachtlová - <https://orcid.org/0000-0002-2833-1528>

Michaela Fecková - <https://orcid.org/0000-0001-6644-3590>

Jan Podlesný - <https://orcid.org/0000-0003-1592-8744>

Milan Klikar - <https://orcid.org/0000-0002-7149-2116>

Patrik Pařík - <https://orcid.org/0000-0002-7434-3116>

Jakub Opršal - <https://orcid.org/0009-0005-5414-5533>

Eliška Juhaňáková - <https://orcid.org/0009-0008-8399-0834>

Veronika Chrtová - <https://orcid.org/0009-0005-5398-2137>

Filip Bureš - <https://orcid.org/0000-0002-2832-6673>

Data Availability Statement

All data that supports the findings of this study is available in the published article and/or the supporting information of this article.

References

- García-Amorós, J.; Maerz, B.; Reig, M.; Cuadrado, A.; Blancafort, L.; Samoylova, E.; Velasco, D. *Chem. – Eur. J.* **2019**, *25*, 7726–7732. doi:10.1002/chem.201900796
- Calbo, J.; Weston, C. E.; White, A. J. P.; Rzepa, H. S.; Contreras-García, J.; Fuchter, M. J. *J. Am. Chem. Soc.* **2017**, *139*, 1261–1274. doi:10.1021/jacs.6b11626
- Jelínková, V.; Dellai, A.; Vachtlová, M.; Fecková, M.; Podlesný, J.; Klikar, M.; Castet, F.; Růžička, A.; Pařík, P.; Pytela, O.; Bureš, F. *J. Photochem. Photobiol., A* **2024**, *449*, 115390. doi:10.1016/j.jphotochem.2023.115390
- Jelínková, V.; Dellai, A.; Verwaerde, L.; Rodriguez, V.; Fecková, M.; Vachtlová, M.; Podlesný, J.; Klikar, M.; Sempé, B.; Hugget, M.; Pařík, P.; Pytela, O.; Castet, F.; Růžičková, Z.; Bureš, F. *Chem. – Eur. J.* **2025**, *31*, e202404221. doi:10.1002/chem.202404221
- Hartley, G. S. *Nature* **1937**, *140*, 281. doi:10.1038/140281a0

6. Zhou, H.; Xue, C.; Weis, P.; Suzuki, Y.; Huang, S.; Koynov, K.; Auernhammer, G. K.; Berger, R.; Butt, H.-J.; Wu, S. *Nat. Chem.* **2017**, *9*, 145–151. doi:10.1038/nchem.2625
7. Feng, Y.; Wei, J.; Qin, L.; Yu, Y. *Soft Matter* **2023**, *19*, 999–1007. doi:10.1039/d2sm01476a
8. Nieborek, M.; Szmigiel, D.; Komorowski, P.; Siemion, A.; Konieczkowska, J.; Schab-Balcerzak, E.; Kozanecka-Szmigiel, A. *Sci. Rep.* **2025**, *15*, 716. doi:10.1038/s41598-024-84884-1
9. Kozanecka-Szmigiel, A.; Hernik, A.; Rutkowska, K.; Konieczkowska, J.; Schab-Balcerzak, E.; Szmigiel, D. *Materials* **2022**, *15*, 8088. doi:10.3390/ma15228088
10. Choi, H. S.; Kim, Y. B.; Lee, C. W.; Kim, H.; Choi, Y.-S.; Kim, D. S. *Sens. Actuators, B* **2025**, *426*, 137058. doi:10.1016/j.snb.2024.137058
11. Ban, J.; Yang, Z.; Pan, L.; Liao, J.; Shi, B. *Iran. Polym. J.* **2025**, *34*, 1375–1386. doi:10.1007/s13726-024-01446-y
12. Cheng, C.-Y.; Chen, C.-W.; Li, C.-C.; Jau, H.-C.; Wang, C.-Y.; Feng, T.-M.; Wei, J.; Yu, Y.; Lin, T.-H. *Adv. Opt. Mater.* **2025**, *13*, 2402565. doi:10.1002/adom.202402565
13. Ishizaki-Betchaku, Y.; Suetsugu, K.; Hara, M.; Nagao, Y.; Matsui, J.; Seki, T.; Nagano, S. *Polym. Int.* **2024**, in press. doi:10.1002/pi.6741
14. Jin, H.; Liu, F.; Wu, P.; Sun, Z.; Sui, P.; Cao, Y.; Zhou, Y.; Lin, S. *Small* **2025**, *21*, 2408147. doi:10.1002/sml.202408147
15. Ren, Z.-H.; Cui, Z.; Li, N.; Yue, X.; Zhang, Y.; Li, P.; Zeng, W.; Guan, Z.-H. *J. Appl. Polym. Sci.* **2025**, *142*, e56629. doi:10.1002/app.56629
16. Zenati, A.; Koirala, K. *Polymer* **2025**, *316*, 127867. doi:10.1016/j.polymer.2024.127867
17. Zhang, Y.; Qiu, Y.; Karimi, A. B.; Smith, B. R. *Eur. J. Nucl. Med. Mol. Imaging* **2025**, *52*, 1576–1595. doi:10.1007/s00259-024-07014-z
18. Dennis, J. M.; Patterson, B. A.; Dolinski, N. D.; Fawcett, S. A.; Lenart, W. R.; Sirk, T. W.; Mrozek, R. A.; Rowan, S. J.; Lenhart, J. L. *Macromolecules* **2025**, *58*, 897–904. doi:10.1021/acs.macromol.4c02191
19. Chen, X.; Jiang, H.; Wang, Y.; Zou, G.; Zhang, Q. *Mater. Chem. Phys.* **2010**, *124*, 36–40. doi:10.1016/j.matchemphys.2010.07.015
20. Chen, X.; Hong, L.; You, X.; Wang, Y.; Zou, G.; Su, W.; Zhang, Q. *Chem. Commun.* **2009**, 1356–1358. doi:10.1039/b820894h
21. Siiskonen, A.; Vesamäki, S.; Priimagi, A. *Beilstein J. Org. Chem.* **2025**, *21*, 1528–1534. doi:10.3762/bjoc.21.115
22. Ndaya, D.; Bosire, R.; Kasi, R. M. *Polym. Chem.* **2019**, *10*, 3868–3878. doi:10.1039/c9py00536f
23. Lameijer, L. N.; Budzak, S.; Simeth, N. A.; Hansen, M. J.; Feringa, B. L.; Jacquemin, D.; Szymanski, W. *Angew. Chem., Int. Ed.* **2020**, *59*, 21663–21670. doi:10.1002/anie.202008700
24. Liu, X.-M.; Jin, X.-Y.; Zhang, Z.-X.; Wang, J.; Bai, F.-Q. *RSC Adv.* **2018**, *8*, 11580–11588. doi:10.1039/c8ra01132j
25. Kamruzzaman, M.; Kim, S.-n.; Kuwahara, Y.; Ogata, T.; Kurihara, S. *Open J. Polym. Chem.* **2013**, *03*, 92–98. doi:10.4236/ojchem.2013.34016
26. Wang, W.; Zhao, N.; Geng, Y.; Cui, S.-B.; Hauser, J.; Decurtins, S.; Liu, S.-X. *RSC Adv.* **2014**, *4*, 32639–32642. doi:10.1039/c4ra06455k
27. Sadler, J. L.; Bard, A. J. *J. Am. Chem. Soc.* **1968**, *90*, 1979–1989. doi:10.1021/ja01010a010
28. Roth, H. G.; Romero, N. A.; Nicewicz, D. A. *Synlett* **2016**, *27*, 714–723. doi:10.1055/s-0035-1561297
29. Zweig, A.; Hodgson, W. G.; Jura, W. H. *J. Am. Chem. Soc.* **1964**, *86*, 4124–4129. doi:10.1021/ja01073a043
30. Haj Said, A.; Matoussi Mhalla, F.; Amatore, C.; Verpeaux, J.-N. *J. Electroanal. Chem.* **1999**, *464*, 85–92. doi:10.1016/s0022-0728(98)00477-x
31. Zeng, C.-C.; Becker, J. Y. *J. Org. Chem.* **2004**, *69*, 1053–1059. doi:10.1021/jo0302253
32. Fischer, E. *J. Phys. Chem.* **1967**, *71*, 3704–3706. doi:10.1021/j100870a063
33. *OPstat*, Version 6.10; Pytela, O.: Pardubice, Czech Republic, 2024.

License and Terms

This is an open access article licensed under the terms of the Beilstein-Institut Open Access License Agreement (<https://www.beilstein-journals.org/bjoc/terms>), which is identical to the Creative Commons Attribution 4.0 International License (<https://creativecommons.org/licenses/by/4.0>). The reuse of material under this license requires that the author(s), source and license are credited. Third-party material in this article could be subject to other licenses (typically indicated in the credit line), and in this case, users are required to obtain permission from the license holder to reuse the material.

The definitive version of this article is the electronic one which can be found at: <https://doi.org/10.3762/bjoc.22.60>